Available online at www.sciencedirect.com
ScienceDirect
Journal of the European Ceramic Society 26 (2006) 3831–3843
www.elsevier.com/locate/jeurceramsoc

Degradation mechanisms of magnesia-chromite refractories by high-alumina stainless steel slags under vacuum conditions

M. Guo *, P.T. Jones, S. Parada, E. Boydens, J.V. Dyck, B. Blanpain, P. Wollants

Department of Metallurgy and Materials Engineering, Katholieke Universiteit Leuven, Kasteelpark Arenberg 44, BE-3001 Leuven, Belgium

Received 17 September 2005; received in revised form 29 November 2005; accepted 9 December 2005
Available online 28 February 2006

Abstract

The corrosion behaviour of magnesia-chromite refractory by an alumina-rich (15–20 wt.%) stainless steelmaking slag is investigated by rotating finger tests in a vacuum induction furnace. The influence on the refractory wear, of the process temperature, corrosion time and, in particular, the high Al_2O_3 content in the slag, is discussed. Two distinct mechanisms cause primary chromite degradation: FeO_x and Cr_2O_3 decomposition because of low oxygen potentials and dissolution by infiltrated slag due to the high Al_2O_3 slag content. Upon decomposition, small metallic particles and pores are homogeneously generated inside the primary chromite. At the refractory/slag interface, a relatively continuous solid $(Mg,Mn)[Al,Cr]_2O_4$ spinel layer is formed. Its density and stability decreases with higher temperatures and more turbulent conditions. The spinel formation arises through heterogeneous in situ precipitation from a slag rich in spinel forming compounds. Higher Al_2O_3 levels in the slag promote the spinel layer formation, which may limit slag infiltration. Finally, it is shown that the present experimental procedure is an excellent tool to simulate refractory wear in industrial processes, diminishing the risks associated with plant trials.

Keywords: Electron microscopy; Corrosion; Spinels; Refractories; Stainless steel slag

1. Introduction

Apart from being the principal refractory material in non-ferrous environments, magnesia-chromite bricks are widely applied in secondary steelmaking applications such as Ruhrstahl Heraeus (RH) degassing units and vacuum oxygen decarburisation (VOD) ladles. Magnesia-chromite refractories are known for their excellent slag resistance, dimensional stability and high hot strength. A multitude of studies on the wear mechanisms of this refractory type have been reported.[1–11] Jones and co-workers[1,2] investigated the degradation mechanisms of magnesia-chromite bricks in VOD applications by post-mortem assessment of industrially worn specimens, corroded by low-Al_2O_3 CaO–SiO–Al_2O_3–MgO–CrO_x slags (<8 wt.% Al_2O_3). Later, these authors used a hybrid microwave heating technique, equipped with quenching facilities, to study the hot-stage microstructures of slag-infiltrated magnesia-chromite specimens recovered from a worn VOD slag lining.[3] Similarly, Mosser et al.[4] observed that magnesia-chromite refractories in RH degassing units suffer from the infiltration of silica-rich or alumina-containing slag into the pores, reaction of the infiltrated slag with the brick matrix, and the subsequent hot erosion of the infiltrated zone.

Some specific studies on the influence of slag basicity on magnesia-chromite wear are also available. Calkins et al.[5] exposed direct-bonded magnesia-chromite refractories to different slags and found that chromite was more resistant than periclase in an acid slag ($CaO/SiO_2 = 0.5$), while periclase was more resistant in basic slags ($CaO/SiO_2 = 2$). Narita et al.[6] confirmed that the corrosion of magnesia-chromite refractories increased with decreasing slag basicity ($B_{\text{basic slag}}$):

$$B_{\text{basic slag}} = \left[\frac{\text{CaO} + \text{MgO}}{\text{SiO}_2 + \text{Al}_2\text{O}_3}\right] \quad (1)$$

with all oxides in wt.%. However, Al_2O_3 often plays an ambiguous role: in an acidic slag it will act as a base affecting basicity in a CaO–SiO–Al_2O_3–MgO slag as follows[12]:

$$B_{\text{acid slag}} = \left[\frac{\text{CaO} + \text{MgO} + \text{Al}_2\text{O}_3}{\text{SiO}_2}\right]. \quad (2)$$

* Corresponding author. Tel.: +32 16 321279; fax: +32 16 321991.
E-mail address: muxing.guo@mtm.kuleuven.be (M. Guo).

0955-2219/$ – see front matter © 2006 Elsevier Ltd. All rights reserved.
doi:10.1016/j.jeurceramsoc.2005.12.025

In this case, Al_2O_3, as a fluxing component, will enhance slag fluidity and thus the penetration potential into the refractory material. On the other hand, it can also reduce the MgO solubility in the slag, decreasing periclase dissolution. More importantly, the slag Al_2O_3 content may influence the corrosion mechanisms of magnesia-chromite refractories by direct or indirect dissolution of periclase. The latter is dependent on whether a dense solid spinel layer forms at the slag/refractory interface at elevated temperatures. Zhang and Lee[13] studied the corrosion of magnesia and predicted the critical condition of $MgAl_2O_4$ (MA) spinel formation through the $CaO–SiO_2–MgO–Al_2O_3$ phase diagrams. Herzog[14] examined the effect of Al_2O_3 content (range from 20 to 40 wt.%) on the corrosion rate of magnesia bricks by a rotary slag test, indicating that in basic slags ($CaO/SiO_2 = 2.3$) refractory corrosion increases with higher Al_2O_3 contents due to direct dissolution of MgO, but in more acid slags ($CaO/SiO_2 = 1.0$), it decreases with increasing Al_2O_3 content because of the indirect dissolution. Clearly, the slag Al_2O_3 content has a great influence on the corrosion mechanisms of magnesia based refractories.

Nevertheless, few systematic studies are available addressing the effect of Al_2O_3-rich $CaO–SiO–Al_2O_3–MgO(–Cr_2O_3)$ slags on the degradation mechanisms of magnesia-chromite refractories in secondary steelmaking applications, such as the VOD process. The investigation of the influence of Al_2O_3 is worthwhile as such slags can be particularly interesting for metallurgical reasons. Elevated Al_2O_3 levels increase the lime solubility and hence the sulphide capacity of the slag, thus improving the desulphurisation process during the production of stainless steel.

In the present paper, the corrosion behaviour of a magnesia-chromite brick by a high Al_2O_3 (15–20 wt.%) $CaO–SiO–Al_2O_3–MgO–Cr_2O_3$ slag is, therefore, investigated. This is done through rotating finger tests in a vacuum induction furnace. The refractory degradation mechanisms are studied by the characterisation of corroded microstructures using scanning electron microscopy energy dispersive spectroscopy (SEM-EDS) and electron probe microanalysis (EPMA) also coupled with EDS. The influence on the refractory corrosion, of exposure time, temperature and, in particular, the high slag Al_2O_3 content, is discussed with respect to the previously reported degradation mechanisms in industrial VOD linings,[1,2] the hybrid microwave studies[3] and other investigations.[4–14]

2. Experimental

2.1. Experimental set-up

Rotating finger tests were performed in a vacuum induction furnace (type VSG 30, 60 kW power supply, 4 kHz frequency). Cylindrical refractory specimens (diameter = 28 mm; length = 202 mm) were dipped into the corrosive slag and liquid stainless steel, and rotated for a certain number of cycles. A schematic diagram of the experimental set-up is shown in Fig. 1a. The detailed experimental conditions are listed in Table 1. An Al_2O_3 crucible (Ø 175 mm × 220 mm) was used to obtain high Al_2O_3 content slags. Approximately 15 kg of stainless steel (AISI 316), 2.6 kg VOD-reduction slags (Table 2) supplied by a stainless steel company and a commercially available top-quality rebonded magnesia-chromite refractory finger (density 3.38 g/cm^3, open porosity 12 vol.%) were employed in the tests. In order to simulate the atmosphere in the VOD process, a gas mixture of CO and CO_2 was blown into the furnace at flowrates of, respectively, 50 and 1 l/min, controlled by a mass-flow meter. The oxygen partial pressure was thus set to be $\sim 10^{-11}$ atm. Three tests were carried out with different temperatures (Test 1:

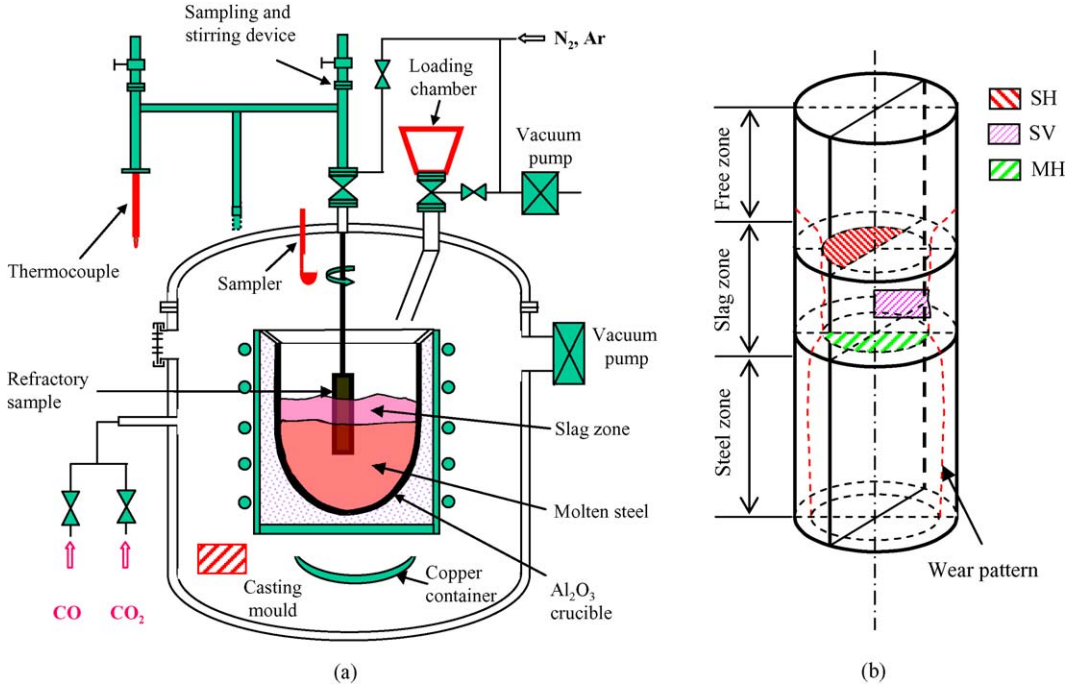

Fig. 1. Schematic diagram of the experimental set-up showing (a) rotating finger test, (b) sample extraction scheme.

Table 1
Experimental parameters

Experiment number	Time (min)	Temperature (°C)	P_{O_2} (atm)	Refractory materials	Other parameters
Test 1	60	1590	1.72×10^{-11}	Rebonded magnesia-chromite	Steel amount: 15 kg
Test 2	120	1610	7.01×10^{-11}		Slag amount: 2.6 kg
Test 3	240	1670	7.20×10^{-11}		Rotating speed: 12 rpm
					Pressure: 5 mbar
					Sample size: Ø 28 mm × 202 mm

1590 °C; Test 2: 1610 °C; Test 3: 1670 °C) and exposure times (respectively 60, 120 and 240 min). In all tests the rotating speed of the refractory finger was 12 rpm.

2.2. Experimental procedure

After charging the stainless steel in the Al_2O_3 crucible, the furnace was evacuated down to approximately 5 mbar. The steel was then heated to the experimental temperature by slowly increasing the furnace power. Heating was commenced at a power of 5 kW, after which the power was increased by 2.5 kW every 10 min until the metal had melted completely (total duration ~2 h). Subsequently, the industrial CaO–SiO–Al_2O_3–MgO–CrO_x slag (Al_2O_3-poor, overall composition in Table 2) was added to the metal through the loading chamber. After the slag was in a fully liquid state, the temperature was regulated to the targeted value by changing the power according to the experimentally determined power–temperature curve.[15] Thereafter, the temperature of the melt was measured by a dip thermocouple (type B: Pt 30%Rh/Pt 6%Rh). For the sake of temperature stabilisation and to obtain a high Al_2O_3 content in the slags (Table 3), the system was held for 60 min at the same power setting. After this period, the temperature was measured once more. Due to the fact that the temperature difference between two consecutive measurements was less than 5 °C, we considered the second measurement as being the obtained temperature. Subsequently, the refractory finger was introduced into the melt. Once the scheduled reaction time was reached, the refractory sample was withdrawn from the furnace and quenched in argon gas. To clarify the temperature gradient in the melt and to better understand the temperature influence on slag/refractory interactions, a temperature profile of the crucible with a charge of 15 kg stainless steel was measured in a separate melting test (Fig. 2).[16]

Table 2
Chemical composition of the (as-delivered) Al_2O_3-poor CaO–SiO–Al_2O_3–MgO–CrO_x VOD slag initially charged in the experiments, as determined by ICP-AES (mass%)

	Average
MgO	13.2
Cr_2O_3	8.1
Al_2O_3	1.8
'FeO'	1.1
CaO	28
SiO_2	45
MnO	1.8
TiO_2	<0.5

Table 3
Composition of slag layers covered on the sample surface after completion of tests, as determined by SEM-EDS (in wt.%)

Sample	MgO	Al_2O_3	Cr_2O_3	SiO_2	CaO	'FeO'
SH1	11.7	17.5	3.5	34	33	<0.5
MH1	11.8	17.9	3.6	33	33	0.7
SV1	12.3	19.5	6.1	31	31	<0.5
SH2	11.4	17.1	3	35	33	<0.5
MH2	12.2	19.1	4.2	34	31	<0.5
SV2	11.4	17.1	3.2	34	34	<0.5
SH3	10.4	15.8	4.1	35	34	<0.5
MH3	11.4	15.6	1.9	37	34	<0.5
SV3	10.2	18.6	4.2	36	31	<0.5

2.3. Microstructural characterisation

Chemical analyses of the initially charged slags (Table 2) were performed with a JEOL 733 electron probe microanalysis (EPMA) system equipped with an energy dispersive spectroscopy (EDS) system (beryllium window) from Tracer. The composition was determined using a semi-quantitative (SQ) EDS routine which serves as an alternative for a more elaborate fully-quantitative wavelength dispersive (WDS)

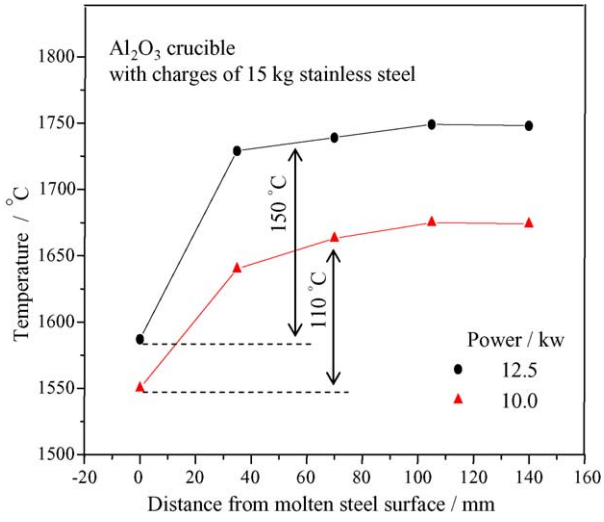

Fig. 2. Temperature profile of the molten steel bath in the experiments.

analysis procedure. This EPMA-EDS procedure requires that the operator selects a priori the oxides (e.g. FeO, Fe_2O_3, Cr_2O_3) or elemental compounds (e.g. Fe, Cr) to be measured, as oxygen (and carbon) cannot be determined directly with this set-up. In order to assess the reliability of the EPMA-EDS method, these results were also compared with inductively coupled plasma atomic emission spectroscopy (ICP-AES), using an accurate and precise analysis procedure (dissolution of slags by hot phosphoric acid digestion).[17]

The recovered cylindrical refractory samples were sliced into three pieces with a diamond saw: the slag zone sample was used for further post-mortem assessment. To evaluate the refractory corrosion behaviour in the different positions along the perpendicular direction to the slag surface, three specimens were prepared from all three slag zone samples. This is demonstrated in Fig. 1b: the three sample types consist of the cross section at the top (SH) and the bottom (MH) parts of the slag zone; and the vertical section at the bottom slag zone (SV). The specimens were embedded in a low viscosity resin (Epofix) by vacuum impregnation, ground with diamond plates and polished with diamond paste. The polished refractory specimens were carbon coated, and characterised using high resolution SEM (Philips XL-30 FEG) equipped with an EDS detector system (from EDAX) with an ultra-thin window, enabling the qualitative identification of elements as light as boron. Additional semi-quantitative analyses were performed using a JEOL 733 EPMA-EDS system.

3. Results and discussion

3.1. Local corrosion

Refractory wear resulting from chemical dissolution of its components into molten slag can be classified into two types: bulk versus local corrosion. Bulk corrosion involves the homogeneous dissolution of the refractory components into the slag phase. Local attack of the refractory can be caused by convection currents at the slag/metal/refractory and/or at the slag/gas/refractory interfaces. The digital image (Fig. 3) illustrates the appearance of the worn samples, showing local corrosion occurred at the slag/metal/refractory and slag/gas/refractory interfaces. The enhanced attack at the slag/metal/refractory interface was believed to be the result of the combined effect of the strong agitation at the slag/metal interface caused by the metal induction, and the Marangoni convection generated by an interfacial tension gradient. As the wettability between slag and brick is larger than that between metal and refractory, a slag film is formed near the refractory/metal boundary. The slag film is in prolonged contact with the brick and subsequently dissolves specific refractory components. As the lower part of the slag film is thinner, the refractory dissolution has a relatively stronger effect on the resulting local slag composition. A chemical gradient thus arises along the slag film, which leads to an interfacial tension gradient that generates the Marangoni flows. On the other hand, a counter current is induced due to the incompressibility of the slag. The refractory surface at the slag/metal interface is continuously exposed to fresh slag; hence the local corrosion takes place due to an effective mass transfer in the slag.[18]

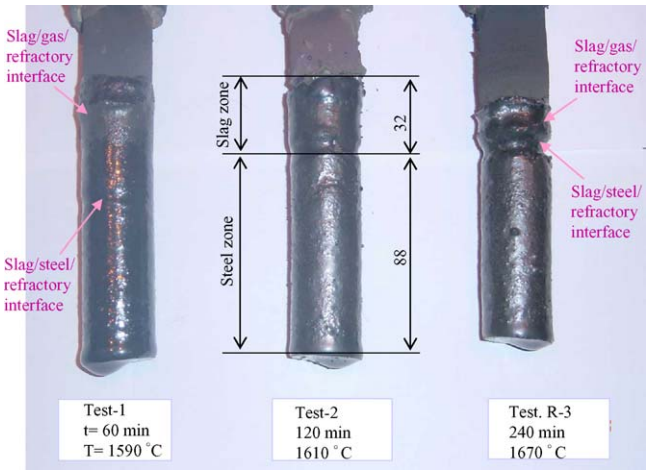

Fig. 3. Digital image of the appearance of worn specimens after the tests, showing local corrosion of magnesia-chromite refractory at the slag/metal interface under different experimental conditions.

As shown in Fig. 3, the local corrosion at the slag/metal/refractory interface was predominant and increased with corrosion time. We used the maximum local corrosion depth, L_m, as a measure to evaluate the extent of the present local corrosion. The values for L_m were measured through SEM images (Tests 1 and 2) of the vertical section specimens or optical measurement prior to sample preparation (Test 3). The results are shown in Fig. 4. Obviously, the maximum local corrosion depth increases with the test duration and temperature. In the case of Test 3 (240 min, at 1670 °C), L_m reached 5 mm. The local corrosion phenomenon was confirmed by industrial observations in VOD linings, as previously reported by the present authors.[19]

3.2. Overview of worn microstructures

Comparing the composition of the initial slag (Table 2) to that of the final slag (Table 3) reveals that the Al_2O_3 levels in the slags increased significantly to values between 15 and

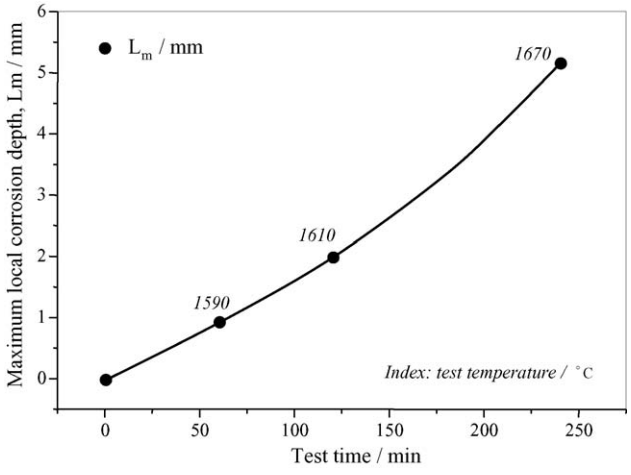

Fig. 4. The change in maximum local corrosion depth at the slag/metal/refractory interface with test time.

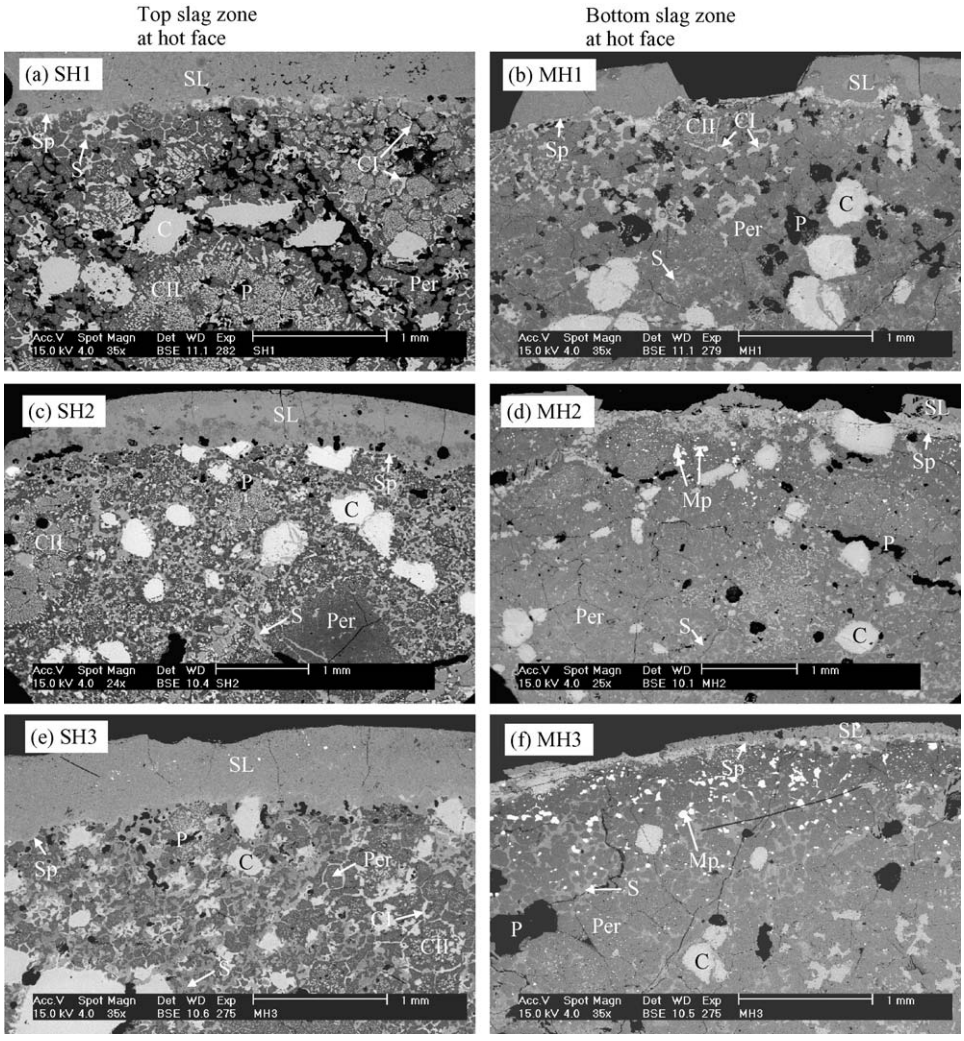

Fig. 5. Overview of worn samples of Tests 1, 2 and 3, showing the hot face at the top (SH1, 2 and 3) and bottom (MH1, 2 and 3) slag zone: Per = magnesia (periclase); C = primary chromite; CI = secondary chromite type I; CII = secondary chromite type II; S = infiltrated slag; Sp = spinel layer; SL = slag layer; Mp = metallic particles; P = pore or crack.

20 wt.%. The refractory samples were subjected to microstructural assessment to understand the refractory wear mechanisms and to evaluate the influence of the experimental parameters. The evolution of the microstructural features for the hot face specimens at both the top (SH1, SH2 and SH3) and bottom (MH1, MH2 and MH3) slag zone are shown in Fig. 5. The corrosion behaviour is characterised by slag infiltration, 'inactivation' of secondary chromite at elevated temperatures and dissolution and decomposition of primary chromite. A relatively continuous spinel layer was observed at the refractory hot face in all top slag zone samples (SH1, SH2 and SH3) and in the bottom slag zone specimen (MH1), whereas a rather loose, fragile spinel layer was found in the other samples (MH2 and MH3). The involved corrosion phenomena will now be described in detail.

3.2.1. Test 1 (1590 °C, 60 min)

Fig. 5a and b are back-scattered electron (BSE) images of the specimens for Test 1 at respectively the top and bottom slag zone. The bottom slag zone sample was completely infiltrated by slag (MH1, Fig. 5b), whereas only a small fraction of slag infiltration was observed in the top slag zone specimen (SH1, Fig. 5a). Accordingly, the top slag zone specimen (SH1) remained almost intact, resembling the as-delivered microstructure in which a large amount of secondary chromite is located both at the periclase grain boundaries and within these grains. A relatively continuous spinel layer was seen at the slag/brick interface in the top slag zone specimen (see further). This presumably protected the brick from major slag infiltration. Although such a relatively continuous spinel layer was also present at the slag/refractory interface in the bottom slag zone specimen (MH1), much less secondary chromite remained. This distinct corrosion level is caused by the temperature gradient along the refractory sample height (vertical direction), which will be discussed later. No FeO_x or Cr_2O_3 decomposition was observed for Test 1.

3.2.2. Test 2 (1610 °C, 120 min)

Test 2 was carried out at a slightly higher temperature and for a longer duration with respect to Test 1, resulting in a considerable modification of the microstructure of the corroded samples, as demonstrated in Fig. 5c (top slag zone, SH2) and Fig. 5d (bottom

slag zone, MH2). The refractory specimens were strongly infiltrated by slag, even in the (cooler) top slag zone sample where a relatively continuous spinel layer could be observed at the refractory/slag interface. The presence of metallic particles indicate that FeO_x or Cr_2O_3 decomposition occurred in the hot face region of the bottom slag zone specimen (MH2). No metallic particles were observed in the top slag zone sample (SH2). The quantity of secondary chromite was considerably lower than it was in Test 1, particularly at the top slag zone. The dissolution of primary chromite into infiltrating slag was clearly observed (Fig. 5c).

3.2.3. Test 3 (1670 °C, 240 min)

As this test incorporated the highest temperatures and longest exposure times, these samples were the most severely degraded, as depicted in Fig. 5e (top slag zone, SH3) and in Fig. 5f (bottom slag zone, MH3). The infiltrated areas inside the brick were more extended while the level of remaining secondary chromite was drastically diminished. In the bottom slag zone it had almost completely disappeared. A substantial number of metallic particles with relatively large size (10–250 μm) were present in the hot face region of the bottom slag zone specimen. Similarly as in Tests 1 and 2, no FeO_x or Cr_2O_3 decomposition occurred at the top slag zone. At the slag/brick interface, however, a relatively continuous spinel layer was observed in the top slag zone sample.

3.2.4. Summary

In brief, findings from Fig. 5 can be summarised as follows: (1) no FeO_x or Cr_2O_3 decomposition occurred in the three top slag zone specimens, whereas it was clearly observed in hot face region of the bottom slag zone specimens MH2 and, even more evident, in MH3, the refractory specimen with the highest temperature and longest exposure time; (2) slag fully penetrated throughout the refractory samples, and almost all the secondary chromite disappeared in the bottom slag zone samples; (3) the dissolution of primary chromite into slags was clearly observed in Tests 2 and 3; and (4) a relatively continuous spinel layer was formed at the slag/brick interface of all top slag zone specimens and in the bottom slag zone specimen MH1; in samples MH2 and MH3 the layer was much less continuous.

3.3. Slag infiltration and MgO dissolution

3.3.1. Slag layer

As seen from Fig. 5, all specimens are covered with a slag layer on their surface, with Al_2O_3 contents ranging from 15 to 20 wt.% (Table 3). This indicates a substantial increase in Al_2O_3 level as compared to the initial charging slag (Table 2), due to Al_2O_3 dissolution from the crucible into the slag. Visual observation of these slag layers (Fig. 5) suggests that there exists a close correlation between the experimental temperature and the thickness of the slag layer. The latter were determined for the bottom slag zone specimens through BSE images: Fig. 6 reveals that there is an inverse relationship between temperature and slag thickness, attributable to the fact that the slag viscosity is inversely related to temperature. In the (cooler) top slag zone

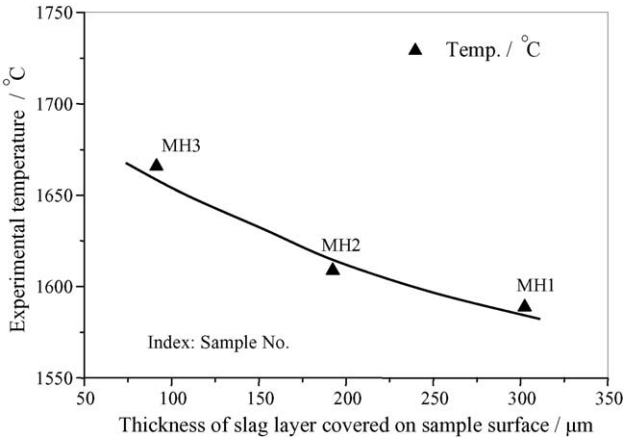

Fig. 6. The relationship between the experimental temperature and the thickness of the slag layers covering the sample surface of the bottom slag zone specimens.

the slags are thus more viscous which implies that they will stick more easily to the refractory surface, thus leaving behind thicker slag layers with respect to the relatively hotter bottom slag zones.

3.3.2. Effect of corrosion time and temperature

The variation of slag infiltration in the brick as a function of test time and temperature is demonstrated in Fig. 7, indicating that with an increase in holding time and temperature, slag infiltration increases substantially. As can be seen in Fig. 7a, the microstructure of the sample centre at the top slag zone remains intact in Test 1 (60 min, 1590 °C). However, with increasing time and temperature, the extent of slag infiltration increased greatly, with a simultaneous decrease in the remaining secondary chromite level (Fig. 7b and c). The periclase and primary grains were heavily attacked by the infiltrating slag in Tests 2 and 3.

As for a given test, the local temperature at the different positions (top or bottom slag zone) is the only variable parameter, the distinct corrosion behaviour is the result of the temperature gradient. To estimate this gradient in the slag zone, the temperature profile measured in previous work can be used (see Fig. 2).[16] It becomes evident that a higher temperature leads to a larger temperature gradient in the melt. In the present experimental temperature range (1590–1670 °C), the temperature of the bottom slag zone was confirmed to be more than 100 °C higher than that of top slag zone. This is in agreement with the observations of the varying slag layer thickness in Fig. 6. Fig. 8 shows the distinct slag infiltration for the different sample positions, which is thus considered to be the direct result of the temperature gradient along the slag zone. As can be seen from Fig. 8a (top slag zone), slag penetrated into the bricks less than 600 μm, whereas at the bottom slag zone (Fig. 8b) an infiltrated network of liquid slag was observed even at the sample centre. This infiltration occurs primarily along the periclase grain boundaries, thereby dissolving MgO from the periclase grains forming 'low melting compounds' which crystallised as $CaO{\cdot}MgO{\cdot}SiO_2$ (CMS) and $3CaO{\cdot}MgO{\cdot}2SiO_2$ (C_3MS_2) during cooling. Elevated temperatures result in deeper slag infiltration, due to the decreased slag viscosity and the 'inactivation' of the (protective) secondary

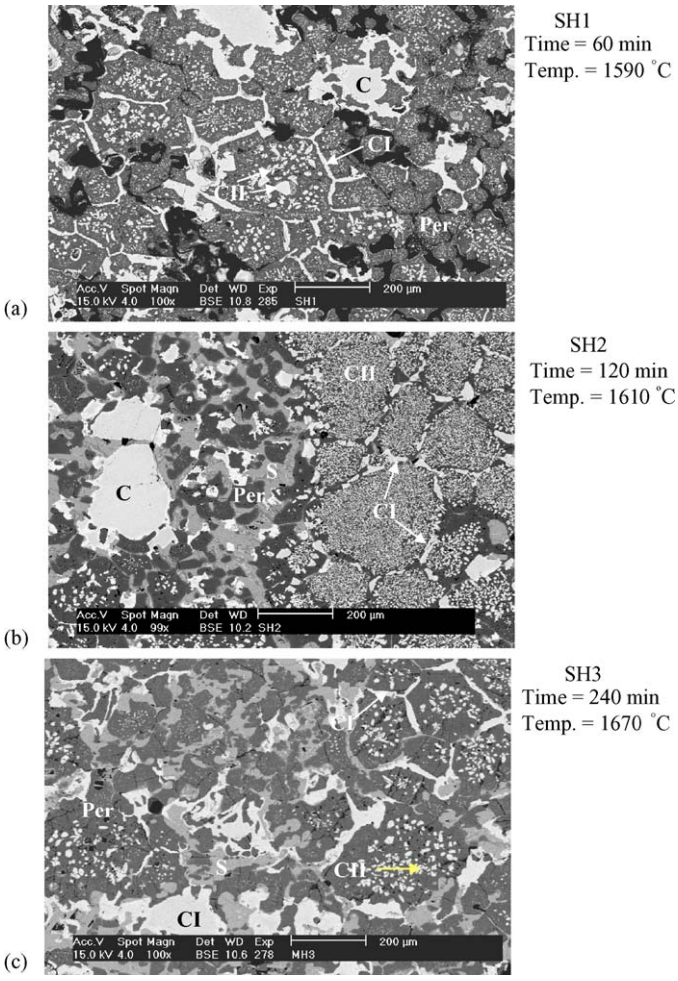

Fig. 7. BSE images of Tests 1, 2 and 3 of the top slag zone specimens in the centre of the samples, showing the time-dependency of the slag infiltration: Per = periclase; S = silicate slag phase; C = primary Chromite; CI = secondary chromite type I; CII = secondary chromite type II.

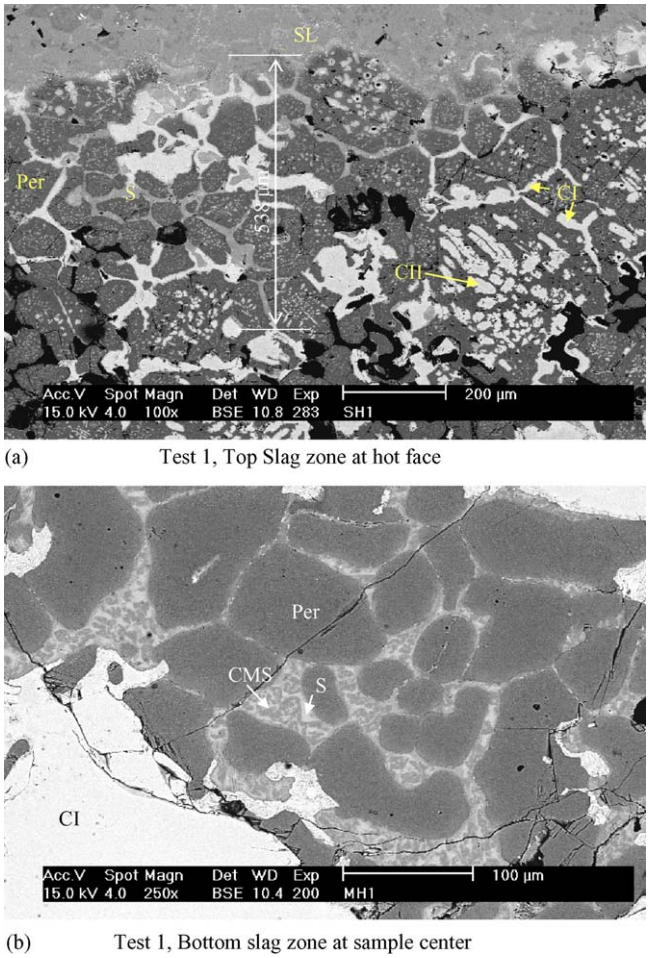

Fig. 8. BSE images of Test 1 at different positions, showing the temperature influence on the behaviour of slag infiltration: Per = periclase; SL = slag layer; S = infiltrated slag; CI = secondary chromite type I; CII = secondary chromite type II.

chromite phases. The latter is caused by its dissolution into both the slag and the periclase solid solution, as previously shown in the hybrid microwave studies of Jones et al.[3] Another reason for the limited slag infiltration observed in Fig. 8a could presumably be attributed to the formation of a relatively continuous spinel layer at the slag/brick interface (see further).

3.3.3. *MgO dissolution from refractory and Al_2O_3 removal from slag*

Refractory dissolution in the slag phase inevitably occurs whenever the infiltrating slag is not saturated with the refractory components. This is confirmed in the present experiments by comparing the compositions of the slag layers attached to the sample hot faces with those of the infiltrated slag inside the brick. Fig. 9a reveals that the MgO content of the infiltrated slag is by average 2 wt.% higher than that of the slag layers on top of the hot faces. On the other hand, the Al_2O_3 content in the slag decreased significantly while infiltrating into the bricks (Fig. 9b). There are several reasons for this. First, part of the slag Al_2O_3 is consumed by the in situ formation of hot face spinel layer (Fig. 12). A second reason is believed to be the result of an ion exchange mechanism between the infiltrated slag and primary (and/or secondary) chromite spinel:

$$(Al^{3+})_{slag} + [Mg^{2+}]_{spinel} = [Al^{3+}]_{spinel} + (Mg^{2+})_{slag} \quad (3)$$

where the square and round brackets represent the spinel and the slag phases, respectively. Al^{3+} ions from the slag enter the primary chromite at the hot face, while Mg^{2+} ions leave the chromite grains. This ion exchange mechanism has been proposed to explain the effect of coal slag on the microstructure of magnesia-chromite refractory.[20] Fe^{3+}/Fe^{2+} ions and Al^{3+} ions reduce the spinel grain melting temperature, a consequence of which is enhanced solution of the refractory in the slag. A third reason for the lower (relative) Al_2O_3 levels in the infiltrated slag is simply due to a dilution effect (through the addition of refractory MgO to the slag).

3.4. *Inactivation of secondary chromite spinel*

The degradation behaviour of secondary chromite phases can be understood from the hot face BSE images of Test 3 as shown in Fig. 10. Secondary chromite is still present together

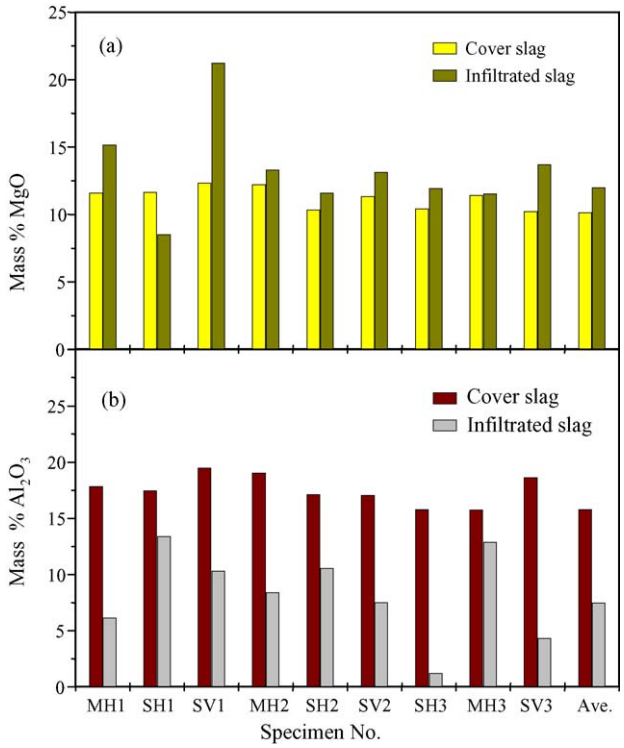

Fig. 9. Comparison of slag composition covering the refractory surface with that of the infiltrated slag in the interior of bricks, as determined by SEM-EDS.

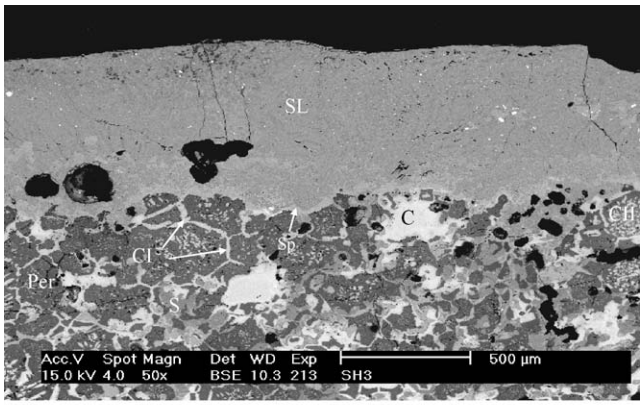

(a) Test 3, top slag zone at hot face

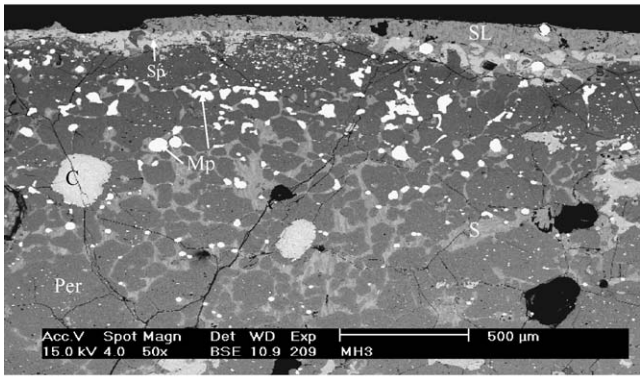

(b) Test 3, bottom slag zone at hot face

Fig. 10. Behaviour of secondary chromite degradation of Test 3 at different positions, showing strong position dependency (temperature difference): Per = periclase; Sp = spinel layer; SL = slag layer; S = infiltrated slag; CI = secondary chromite type I; CII = secondary chromite type II; C = primary chromite; Mp = metallic particles.

with the infiltrated slag in the top slag zone sample (Fig. 10a), whereas almost all of it disappeared in the hotter bottom slag zone specimen (Fig. 10b). Since for a given test, except for the temperature gradient, there are no differences as regards to the experimental parameters in the slag zone, it is inferred that the higher temperature imposed on the bottom slag zone effectively activated the diffusion of the components of secondary chromite into the surrounding periclase solid solution and/or its dissolution into the infiltrated slag. This leads to its disappearance in the refractory microstructure and confirms the mechanism as 'secondary chromite inactivation'.[3] A two-phase direct-bonded microstructure (periclase + chromite) is transformed into a much weaker single-phase, liquid-bonded structure, which subsequently accelerates slag infiltration.

3.5. Degradation of primary chromite spinel

Two primary chromite degradation mechanisms were observed in the present experiments: (1) infiltrated slag dissolves primary chromite grains (Fig. 11a) and (2) FeO_x or Cr_2O_3 decomposition occurs at elevated temperatures (Fig. 11b). The latter was only observed in the bottom slag zone samples, which implies that temperature strongly affects the decomposition behaviour. In general, the chemical decomposition of FeO_x and Cr_2O_3 can be expressed, respectively, as:

$$\mathrm{FeO\,(s)} = \mathrm{Fe\,(l)} + \tfrac{1}{2}\mathrm{O_2\,(g)}; \quad \Delta G_3^\circ = 287340 - 73.7T \qquad (4)$$

$$\mathrm{Cr_2O_3\,(s)} = 2\mathrm{Cr\,(s)} + \tfrac{3}{2}\mathrm{O_2\,(g)}; \quad \Delta G_4^\circ = 1110000 - 247T \qquad (5)$$

where ΔG_3° and ΔG_4° are the standard Gibss free energy changes expressed in J/mol[21] for respectively FeO_x (expressed as 'FeO') and Cr_2O_3 decomposition. The FeO_x or Cr_2O_3 decomposition process is determined by the temperature, the oxygen potential and the activities of FeO_x or Cr_2O_3 in the primary chromite spinel. Note that this phenomenon also takes place in the periclase solid solution phase. Due to the fact that the activities are predetermined in a given refractory and the oxygen partial pressure was fixed to be 10^{-11} atm in the furnace, temperature was the only operational variable in the present tests. The present results indicate that the decomposition occurs as the actual temperature of refractory exposure is in excess of 1600 °C (MH2: 1610 °C; MH3: 1670 °C). Fig. 11b shows the oxide decomposition process in the primary chromite grains. A substantial number of small metallic droplets (<1 μm) are located in the primary chromite matrix. This suggests that as a result of the low oxygen pressure and the high temperature, the decomposition started from the nucleation of liquid droplets along the cracks and pores in the interior of the chromite crystals, followed by growth of the droplets with further decomposition. Finally, these droplets merged together, forming larger size metal phases. As

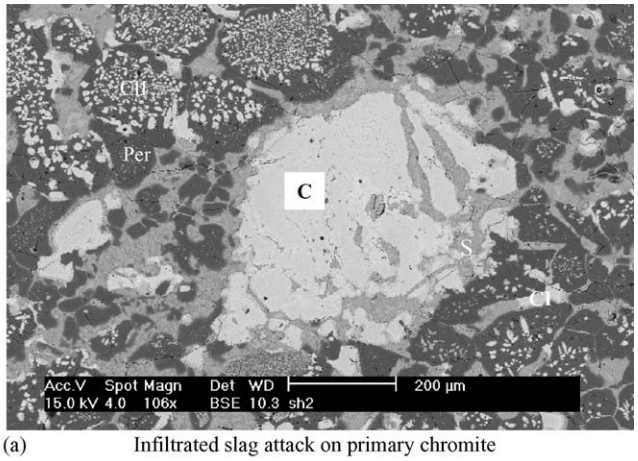

(a) Infiltrated slag attack on primary chromite

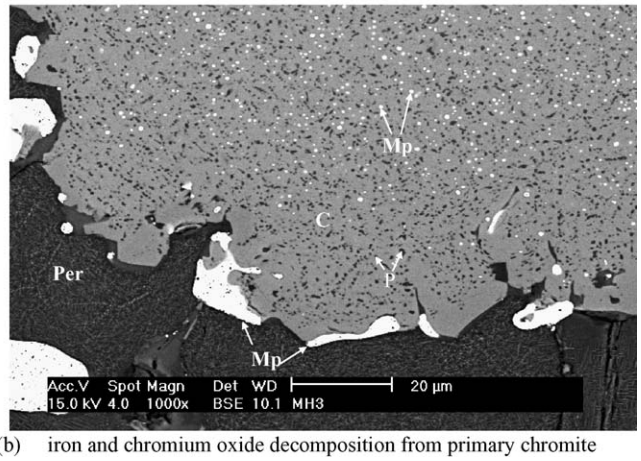

(b) iron and chromium oxide decomposition from primary chromite

Fig. 11. Degradation mechanism of primary chromite, showing (a) slag attack on a primary chromite crystal and (b) iron and chromium oxide decomposition inside a primary chromite grain: Per = periclase; S = infiltrated slag; CI = secondary chromite type I; CII = secondary chromite type II; C = primary chromite; Mp = metallic particles; P = pore or crack.

the decomposition proceeds, a large number of labyrinth-like pores or cracks were formed in the chromite matrix as a result of volumetric shrinkage associated with the decomposition reactions. The shrinking further facilitates both the nucleation of metallic droplets and the removal of oxygen gas (from the reaction site) generated during the decomposition. Table 4 gives an overview of the compositional changes of the primary chromite

Table 5
Composition of metallic particles resulting from refractory decomposition, as determined by SEM-EDS (in mass%)

Sample	Cr	Fe	Remarks
MH2	12.6	86.9	No decomposition occurs in Test 1 (SH1, MH1), and in top slag zone of Tests 2 and 3 (SH2, SH3) (see Fig. 5)
SV2	11.3	88.7	
MH3	1.9	98.1	
SV3	22.3	77.7	

for distinct levels of decomposition. The compositions of the primary chromite of the as-delivered bricks[22] are also listed there for comparing the changes. The presence of metallic particles is associated with a significant decrease in FeO_x content in the chromite matrix. The metallic droplets resulting from the decomposition of the primary chromite crystals are rich in iron (>80 wt.%) with smaller levels of chromium (<20 wt.%), indicating that FeO_x decomposition is more predominant than Cr_2O_3 decomposition (Table 5). This is consistent with the results shown in Table 4 (low FeO content in the primary chromite with metallic particles) and previous findings.[1–3] The preferential decomposition of FeO_x is mainly due to the lower standard Gibbs free energy value for FeO_x decomposition than that for Cr_2O_3 at the present temperature (see Eqs. (4) and (5)). The decomposition phenomenon enhances further slag infiltration and its reaction with the chromite components, which accelerates the wear of the primary chromite grains.

As regards to the direct dissolution of primary chromite into the infiltrating slag, attention should be paid to the slag composition. Because of the amphoteric character of Al_2O_3, an increase in the Al_2O_3 level in the present relatively acidic slag (Table 3) results in (1) a higher slag basicity, thus decreasing the slag resistance of chromite, and (2) a more fluid slag (Al_2O_3 behaves as a network modifier in this case), facilitating slag infiltration. This leads to more elevated primary chromite dissolution. This finding is confirmed by the experiments of Demir and Eric[12] who reported that increasing the Al_2O_3 to CaO ratio in the slag results in an increased dissolution rate of chromite. The dissolution of primary chromite into the slag is also enhanced as Al^{3+} ions reduce the primary spinel grain melting temperature.[20] Within the refractory, the Al^{3+} and Fe^{2+} ions leave the penetrating slag to be replaced by Cr^{3+} and Mg^{2+} ions, which changes

Table 4
Composition of primary chromite phases under different conditions, as determined by SEM-EDS (in mass%)

Sample	MgO	Al_2O_3	Cr_2O_3	'FeO'	Note
MH1	20.5	17.0	52	10.5	Without decomposition (no metallic particles in primary chromite)
SH1	18.0	17.2	56	8.8	
SH2	20.4	16.7	51	11.8	
SH3	21.2	17	49	12.5	
MH2	20.7	19.2	58	2	With decomposition (major presence of metallic particles)
MH3	23.2	17.6	54	5	
As-del.[a]	18.3	15.9	52	11	As-delivered bricks with heating to different temperature and rapid quenching to room temperature
1500 °C[a]	18.0	14.5	53	14	
1600 °C[a]	18.6	15.7	53	12	
1700 °C[a]	17.0	15.0	53	13	

[a] Jeol 733 EPMA-EDS (semi-quantitative) data cited from Ref. 22.

the melt composition from resembling that of anorthite (CAS_2) to diopside (CMS_2). Because of this change in composition the viscosity of the intergranular slag in the refractory is lowered rendering it more reactive.

3.6. Spinel formation

High-temperature dissolution of MgO into CaO–MgO–SiO_2–Al_2O_3(–Cr_2O_3) slags can be direct or indirect, depending on whether a spinel layer forms at the magnesia/slag interface. In the present experiments, the latter phenomenon took place in all samples, albeit to a varying extent depending on the actual conditions. Fig. 12 gives an overview of the (Mg,Mn)[Al,Cr]$_2O_4$ spinel layers for the six different specimens. From these images one may conclude that the layer is relatively continuous in the samples of Test 1 (lowest temperature, SH1 and MH1) and in the top slag zone samples of Test 2 (SH2) and Test 3 (SH3). On the other hand, in the samples MH2 and MH3 the spinel layer is less continuous, with fewer points of contact. Note the striking difference in composition between the in situ formed (Mg,Mn)[Al,Cr]$_2O_4$ spinel phases (e.g. SH3 and MH3, Table 6) compared to the original refractory chromite spinel phase in the as-delivered bricks, i.e. (Mg,Fe^{2+})[Cr,Al,Fe^{3+}]$_2O_4$ (see also Table 6). The latter contains not only a higher amount of Cr_2O_3 with respect to Al_2O_3 but also consists of a considerable level of FeO_x while MnO is not present in any meaningful quantities.

Three potential explanatory schemes can be put forward to clarify the present spinel layer formation mechanism: (a) in situ conversion of the refractory hot face by reaction with liquid slag components, (b) spinel precipitation from the slag upon cooling, and (c) in situ high-temperature spinel precipitation. Mechanism (a) can be definitely ruled out by thorough investigation of the refractory/slag interfaces. Fig. 13 presents detailed images of the relatively continuous spinel layer at the hot face of SH3. These micrographs demonstrate that the phase is not only present at the magnesia/slag interface (Fig. 13a), but can also be seen on isolated primary chromite grains exposed to the slag phase (Fig. 13b). Likewise, Fig. 13 reveals that the spinel phase is also present in the slag as a network of angular grains, contacting the relatively dense spinel layer on top of the refractory hot

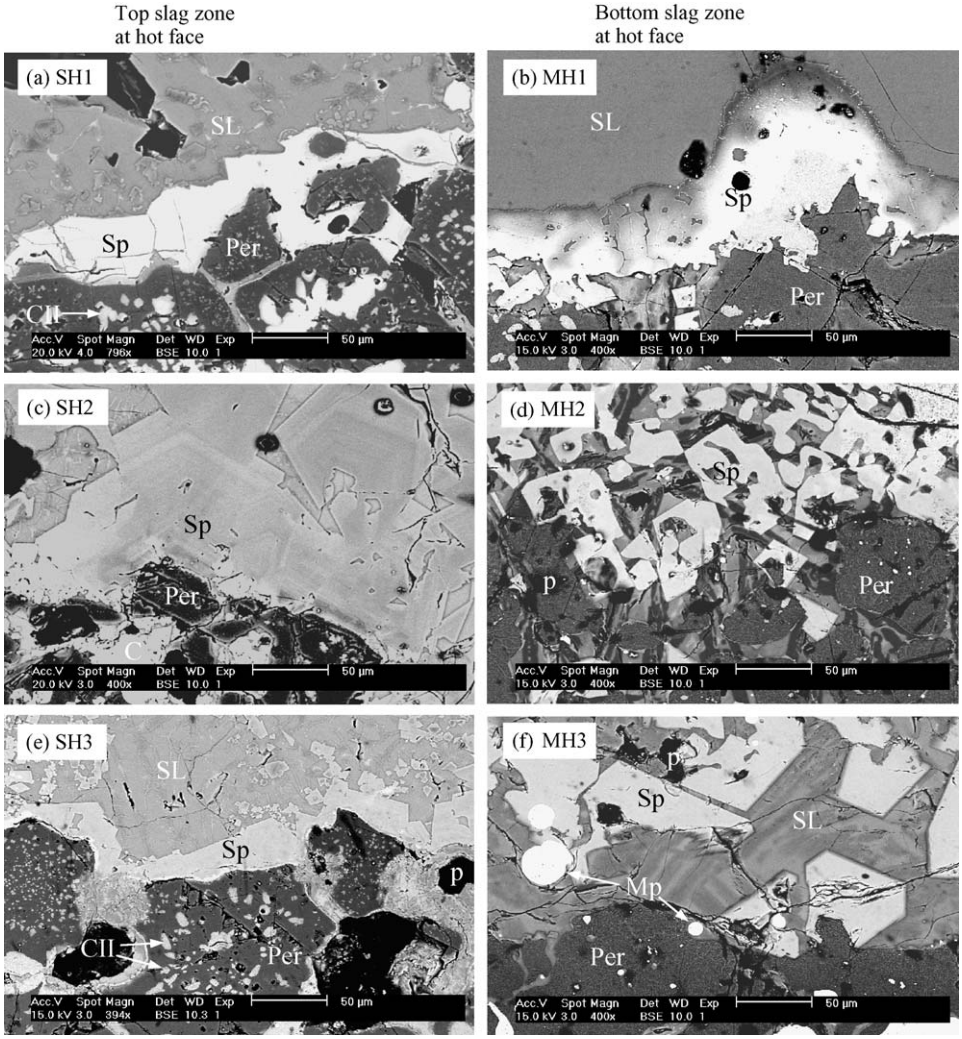

Fig. 12. Spinel layer formation at the slag/refractory interface for the different samples, showing a relatively continuous layer for SH1, SH2, SH3 and MH1, while a less continuous one for MH2 and MH3: Per = periclase; C = primary chromite; Sp = spinel layer; SL = slag layer; Mp = metallic particles; P = pore or crack.

Table 6
Composition of the spinel in SH3 and MH3 and the original primary and secondary chromite phases, as determined by EPMA-EDS (oxides in wt.%, elements in at% between brackets)

Sample	MgO	Al_2O_3	Cr_2O_3	'FeO'	MnO	Position
MH3	23.5 (14.1)	27.6 (13.1)	46.9 (14.9)	0.5 (0.2)	<0.5	Spinel layer on periclase
SH3	22.8 (13.3)	36.9 (17.0)	38.1 (11.8)	0.5 (0.2)	1.1 (0.4)	Spinel layer on periclase
SH3	22.8 (13.4)	33.7 (15.7)	39.8 (12.4)	0.5 (0.2)	1.7 (0.6)	Spinel layer on primary chromite grain
SH3	23.6 (13.6)	39.3 (17.8)	34.1 (10.4)	0.4 (0.1)	1.4 (0.5)	the angular spinel grain network
As-del (II)[a]	21.0	15.1	42.0	20.0	<0.5	Original secondary chromite
As-del (I)[a]	18.3	15.9	52.0	11.0	<0.5	Original primary chromite

[a] Data cited from Ref. 22.

face. EPMA-EDS spot analyses were performed in these three different positions. Results shown in Table 6 reveal that the composition of the spinel layer on both the magnesia/periclase grains and the primary chromite crystals (and the angular spinel grain network) is almost identical, which is an indication that a single mechanism is responsible for the formation of both the hot face spinel layer and the angular spinel grain network in the slag. The spinel must thus be the result of a precipitation phenomenon from the slag, either during cooling or in situ. In the following, we demonstrate that mechanism (b) (precipitation during cooling) should be rejected in favour of mechanism (c) (in situ formation). This is supported by the fact that the spinel precipitation only occurred in a narrow region along the refractory/slag interface rather than in the bulk slag. Fig. 14 clearly demonstrates that there is an abrupt boundary between the hot face region containing spinel crystals and the bulk slag which is completely free of spinel grains. If the precipitation had occurred during cooling, the spinel grains would have been scattered along the refractory hot face towards the bulk slag without such a distinct spinel/slag

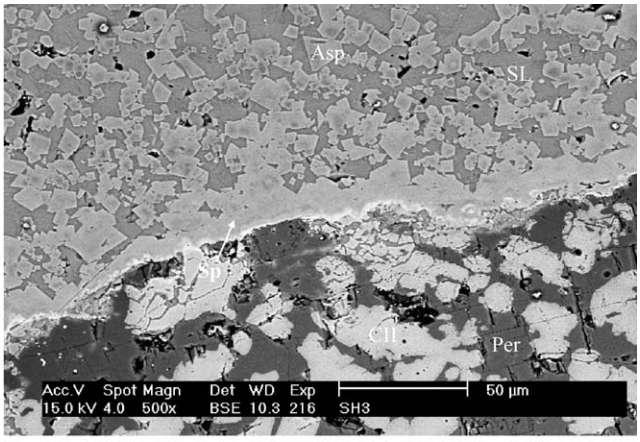

(a) On top of magnesia/periclase grains (SH3, Test 3, at top slag zone)

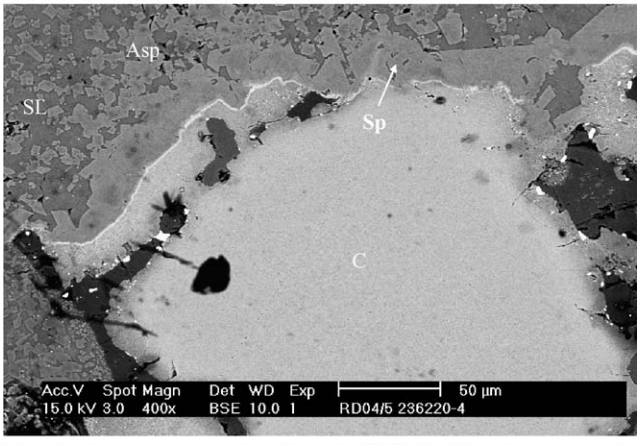

(b) On top of a primary chromite grain (SH3, Test 3, at top slag zone)

Fig. 13. Detailed images of the relatively continuous spinel layers formed at the refractory/slag interface of SH3 on top of (a) periclase grains and (b) a primary chromite grain: Per = periclase; SL= slag layer; CII = secondary Chromite type II; Sp = spinel layer; Asp = the angular spinel grain network.

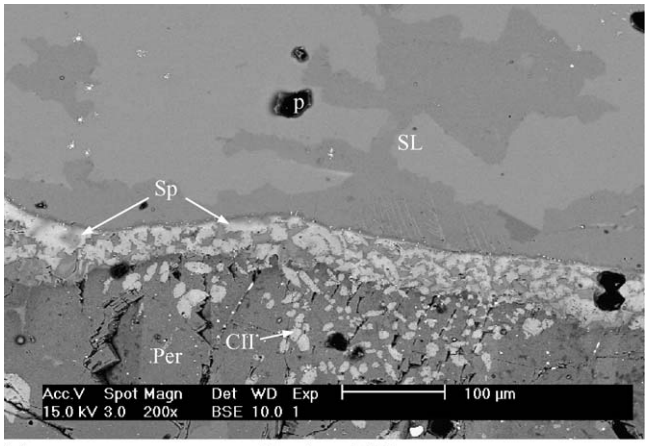

(a) Specimen MH1

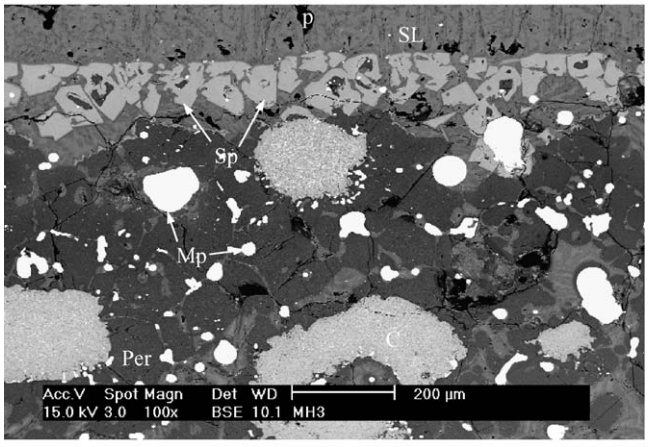

(b) Specimen MH3

Fig. 14. SEM images of (a) MH1 and (b) MH3, showing the in situ formed spinel layer at the refractory/slag interface and the distinct spinel region/bulk slag boundary: Per = periclase; SL = slag layer; C = primary chromite; CII = secondary Chromite type II; Sp = spinel layer; Mp = metallic particles; P = pore or crack.

boundary. Therefore, the spinel must have been formed in situ through precipitation from the local slag at test temperatures. The microstructure shown in Fig. 14 can be considered as being the actual high-temperature state of the refractory hot face, arising during the rapid argon cooling of the sample in the quenching chamber after withdrawal from the furnace.

Both thermodynamic and kinetic aspects are involved in its formation as, respectively, the slag is saturated in spinel forming compounds and, concurrently, the rough refractory hot face kinetically facilitates heterogeneous nucleation of spinel, resulting in a relatively continuous layer along the refractory hot face. The existence of a thermodynamic driving force for spinel formation is consistent with the phase diagram analysis of Zhang and Lee[13] who reported that, to form a $(Mg)[Al]_2O_4$ spinel layer at high temperature, the Al_2O_3 content in a $CaO–MgO–SiO_2–Al_2O_3$ slag should be in excess of 10 wt.%. As in the present case, the local slag close to the refractory hot face is not only saturated with MgO (dissolving from periclase), but also consists of a substantial amount of an additional spinel forming compound (i.e. 2–6 wt.% Cr_2O_3) and contains 15–20 wt.% Al_2O_3, it should be clear that there exists a major driving force for spinel formation.

The difference in amount and density of the observed spinel layers in the distinct specimens is due to differences in temperature, slag viscosity and turbulence. The bottom slag zone parts were exposed to higher temperatures and stronger levels of turbulence (see above) with respect to the top slag zone. Higher temperatures bring about lower slag viscosities and also increase the solubility of the spinel compounds in the slag, while higher levels of turbulence render it more difficult for stabilising a continuous spinel layer formation on top of the refractory surface. This explains why the slag layer is much less continuous in MH2 (∼1610 °C) and MH3 (∼1670 °C) than in the cooler and low turbulence samples: SH1 (∼1490 °C), SH2 (∼1510 °C) and SH3 (∼1570 °C). The latter temperatures were estimated by taking the temperature gradient along the vertical direction of the slag zone into account (Fig. 2).

To conclude this spinel section, it can be stated that the experimental temperature and the level of turbulence are, besides slag composition (Al_2O_3 content and *C*/*S* ratio), the important influencing factors. From this we may understand the critical conditions for its formation. Increasing the Al_2O_3 content will generally favour the precipitation of spinel at elevated temperature. However, as discussed in Section 3.5, the high Al_2O_3 content of the slag also enhances the degradation of the primary chromite in the refractories. Further investigation is, therefore, required to understand the net influence of Al_2O_3 on the overall refractory wear.

4. Conclusions

In order to simulate refractory wear in Al_2O_3-rich stainless steelmaking slags, rotating finger tests were performed in a vacuum induction furnace. Magnesia-chromite refractory samples were brought into contact with $CaO–SiO–Al_2O_3–MgO–Cr_2O_3$ slags containing 15–20 wt.% Al_2O_3. Microstructural characterisation allowed to study the influence of the experimental temperature and, more specifically, the Al_2O_3 content of the slag on the refractory/slag interactions. The following conclusions can be drawn:

(1) Local corrosion was especially observed at the slag/metal interface, particularly in the test with the longest and hottest exposure conditions. It is presumed to be the combined effect of Marangoni flows and agitation at the slag/metal interface caused by steel induction. Slag infiltrates the refractory finger through the open pore network and along the periclase grain boundaries. The infiltration increases with corrosion time and temperature. High temperature inactivation of secondary chromite phases enhances this process considerably.
(2) Primary chromite degradation takes place according to two distinct mechanisms: FeO and Cr_2O_3 decomposition and dissolution by infiltrated slag. The former occurs because of low oxygen potentials and high temperatures, whereas the latter is enhanced by the high Al_2O_3 content of the slag. During decomposition, small metallic particles and pores are generated, which form homogeneously inside the primary chromite.
(3) FeO_x and Cr_2O_3 decomposition may also proceed in the periclase solid solution phase when temperatures are in excess of 1600 °C. This results in a further destabilisation of the refractory hot face, possibly inducing peeling and/or spalling mechanisms.[1–3]
(4) A relatively continuous solid spinel layer was observed at the refractory/slag interface for all top slag zone samples, where temperature and turbulence level are lower than in the bottom slag zone samples. The density and stability of this $(Mg,Mn)[Al,Cr]_2O_4$ spinel layer decreases with higher temperatures and more turbulent conditions. The spinel formation arises through heterogeneous in situ precipitation from the (local) slag which is rich in spinel forming compounds, i.e. Al_2O_3 (15–20 wt.%), Cr_2O_3 (2–6 wt.%) and MgO (>12 wt.%). Higher Al_2O_3 levels in the slag promote the spinel layer formation. These spinel layers are believed to help protect the bricks from severe slag infiltration. Industrial conditions may, however, be too turbulent to maintain the integrity of these passivating layers.
(5) The present tests suggest that high Al_2O_3 contents in relatively acidic $CaO–SiO–Al_2O_3–MgO–Cr_2O_3$ slags lead to a poorer slag resistance of chromite spinel in magnesia-chromite refractories with reference to Al_2O_3-poor stainless steelmaking slags.[1–3] On the other hand, these slags with high Al_2O_3 contents favour the formation of solid spinel at high temperature which may retard slag infiltration. Since the relative influence of these two mechanisms on the overall refractory wear in an industrial steelmaking environment (e.g. VOD process) have not been fully assessed, follow-up studies can be of interest.
(6) Finally, many mechanisms seen in industrial reality are also observed in the present laboratory experiments. The advantage of the lab set-up, however, lies in the possibility to target the investigation of the influence of specific parameters. The present experimental procedure is, there-

fore, an excellent tool for the in-depth study and simulation of refractory degradation mechanisms in industrial metallurgical processes, allowing to diminish the risks associated with industrial plant trials.

Acknowledgements

This work was performed with the financial and technical support of U&A Belgium and the IWT (project no. 990348). The authors thank the engineers of U&A Belgium and PVA for their close co-operation with our team. Practical advice from Heraeus Electro-Nite and Jacques Cortier (Dyson Refractories) were much appreciated.

References

1. Jones, P. T., Blanpain, B., Wollants, P., Hallemans, B., Heylen, G. and Weytjens, J., Extending the lining life of ALZ nv's ladle lining. *Iron Steelmak.*, 1999, **26**(12), 31–35.
2. Jones, P. T., Blanpain, B., Wollants, P., Ding, R. and Hallemans, B., Degradation mechanisms of magnesia-chromite refractories in vacuum-oxygen decarburisation ladles during the production of stainless steel. *Ironmak. Steelmak.*, 2000, **27**, 228–237.
3. Jones, P. T., Vleugels, J., Volders, I., Blanpain, B., Van der Biest, O. and Wollants, P., A study of slag-infiltrated magnesia-chromite refractories using hybrid microwave heating. *J. Eur. Ceram. Soc.*, 2002, **22**, 903–916.
4. Mosser, J., Buchebner, G. and Dösinger, K., New high-quality MgO-Cr_2O_3-bricks and Cr-free alternatives for the lining of RH/DH-vessels. *Veitsch-Radex Rundshau*, 1997(1), 11–23.
5. Calkins, D. J., Gilbert, V. and Saccomano, J. M., Refractory wear in the argon–oxygen decarburization process. *Ceram. Bull.*, 1973, **52**(7), 570–574.
6. Narita, K., Onoye, T., Satoh, Y. and Tanikchi, K., Slag testing of refactories for ladle refining by ESR method. *Taikabutsu (Refractory)*, 1984, **36**, 273–277.
7. Whitworth, D. A., Jackson, F. D. and Patrick, R. F., Fused basic refractories in the argon–oxygen decarburization process. *Ceram. Bull.*, 1974, **53**, 804–808.
8. Takahashi, H., Kawakami, T., Oguchi, Y. and Tsuchiya, I., Application of high Cr_2O_3 magnesia chrome refractories to secondary refining systems. *Taikabutsu (Refractory)*, 1988, **40**, 564–566.
9. Kyoden, H., Ichikawa, K. and Iwado, H., Texture and slag resistance of commercial fused magnesia-chrome clinker. *Taikabutsu (Refractory)*, 1985, **37**, 284–290.
10. Engel, R., Marr, R. and Pretorius, E., Refractory/slag systems for ladle and secondary refining processes. *Iron Steelmak.*, 1997, **24**(4), 59–60.
11. Leonard, R. J. and Herron, R. H., Volume expansion and structural damage in periclase-chrome refractories. *Ceram. Bull.*, 1972, **51**, 891–895.
12. Demir, O. and Eric, R. H., Dissolution of chromite in liquid slag: Empirical relationship. In *Proceedings of the 6th International Conference on Molten Slags, Fluxes and Salts*, 2000.
13. Zhang, S. and Lee, W. E., Use of phase diagrams in studies of refractory corrosion. *Int. Mater. Rev.*, 2000, **45**(2), 41–58.
14. Herzog, S. P., On the formation of protective spinel layers on refractories. *Scand. J. Metall.*, 1976, **5**, 145–150.
15. Guo, M., Van Dyck, J., Parada, S., Jones, P. T., Blanpain, B. and Wollants, P., Laboratory set-up to study refractories in VOD process conditions. *ATB Metall.*, 2003, **42**(3/4), 3–9.
16. Guo, M., Parada, S., Smets, S., Jones, P. T., Van Dyck, J., Blanpain, B. and Wollants, P., Laboratory study of the interaction mechanisms between magnesia-chromite refractories and Al_2O_3-rich VOD slags. In *Proceedings of the VIIth International Conference on Molten Slags, Fluxes and Salts*, 2004, pp. 327–336.
17. Jones, P. T., Hallemans, B., Blanpain, B. and Wollants, P., Optimisation of an accurate and precise and analysis procedure for metallurgical VOD slags with ICP-OES. *Atom. Spectrosc.*, 2000, **21**(3), 86–92.
18. Tao, Z., Mukai, K. and Ogata, M., Local corrosion of magnesia-chromite refractory at slag-metal interface. *Taikabutsu Overseas*, 1999, **19**, 3–10.
19. Jones, P. T., Degradation mechanisms of basic refractory materials during the secondary refining of stainless steel in VOD ladles. PhD Thesis, Leuven, 2000, Chapter VIII, 23.
20. Zhang, S. and Lee, W. E., Melt corrosion of oxide and oxide-carbon refractories. *Int. Mater. Rev.*, 1999, **44**(3), 77–104.
21. Engh, T. A., *Principles of Metal Refining*. Oxford University Press, Oxford, 1992, p. 407.
22. Jones, P. T., Degradation mechanisms of basic refractory materials during the secondary refining of stainless steel in VOD ladles. PhD Thesis, Leuven, 2000, Chapter VII, 6.